M&C 2017 - International Conference on Mathematics & Computational Methods Applied to Nuclear Science & Engineering, Jeju, Korea, April 16-20, 2017, on USB (2017)

CFD Simulation of a 61-pin Wire-wrapped Fuel Subassembly for Sodium Cooled Fast Reactor

Jing Chen✉, Dalin Zhang, Xinan Wang, Suizheng Qiu, G.H. Su, Yapei Zhang

School of Nuclear Science and Technology, State Key Laboratory of Multiphase Flow in Power Engineering, Xi'an Jiaotong University, No.28 Xianning West Road, Xi'an, P.R. China, 710049, Corresponding email: c.j.8902199@stu.xjtu.edu.cn

Abstract - *China Experimental Fast Reactor(CEFR) is the first step of China sodium cooled fast reactors (SFRs) development followed by the demonstration reactor CFR600. The thermal hydraulics behavior of the coolant in helical wire-wrapped fuel subassemblies is of great significance in the design and safety operating of SFRs. However, geometric complexities created by wire spacers bring significant modeling difficulties. In the present study, structured mesh for the wire-wrapped fuel bundle is generated using a special mesh marked and separated method. A validation study is firstly performed to compare the numerical results of a 19-pin wire-wrapped fuel assembly with experiment data reported in the literature. And then CFD simulation with the realizable k–ε turbulence model, for investigating the heat-generating 61-pin fuel subassembly of CEFR, has been carried out. Three-dimensional sodium flow and temperature nonuniformity phenomena in the fuel subassembly were obtained and quantitatively analyzed. Results indicate that the coolant velocity in the subassembly exhibits periodic oscillations. The complex axial and transverse flow behaviors vary in different types of subchannels. The average axial velocity in the edge and corner subchannels is about 23% higher than that in the interior subchannel. Wire wrappers induce a transverse flow of up to about 30% of the axial velocity..*

I. INTRODUCTION

The global economic development brings increasing energy demand. Meanwhile, much attention has been devoted to environmental issues caused by the slather of traditional fossil resources, such as serious air pollution and green house effect. Nuclear power plays an important role in the solution of long term and clean energy requirements. Sodium cooled fast reactor (SFR), which is one of the fourth generation reactor systems, has remarkable advantages in the utilization of natural uranium, management of high-level wastes and transmuting long-lived actinides, as well as good economic benefit. The SFR is recommended as prior development reactor in the Generation IV International Forum (GIF).

The SFRs development strategy in China follows three steps: experimental fast reactor, demonstration fast reactor and commercial fast reactor[1]. As the first step, China Experimental Fast Reactor(CEFR) was launched conceptual design in 1990 and achieved the first physical criticality in 2010[2]. CEFR is a 65MWth and 20MWe pool-type SFR firstly loaded with uranium oxide fuel and then mixed uranium-plutonium oxide. The demonstration reactor CFR600 is followed and designed on the basis of safety requirements of the Generation-IV reactor system [3]. Fuel subassemblies, featured with a large number of closely packed fuel pins and helical wire-wrapped spacers, are predominantly adopted in SFRs. Determination of the peak cladding temperature depends on accurate simulation of the coolant velocity and temperature distribution in the fuel subassembly. The complex radial and axial flow effects highly dependent on the geometry of wire-wrapped bundles. However, in the dense and elongated bundle subchannels, helical wire-wrapped spacers are nearly tangent to fuel pin surfaces, which brings significant modeling difficulties[4].

There has been an increasingly growth in the number of CFD investigations on the flow and temperature fields in the subassemblies of SFRs recently. Pointer et al. (2009)[5] predicted flow fields and temperature profiles for different pin fuel assemblies utilizing the RANS models and considered impacts of alternate meshing methods. Kurt D. Hamman and Ray A. Berry (2010)[6] investigated a CFD modeling and simulation (M&S) process of a 19-pin fast reactor fuel assembly with an effort to resolve the momentum boundary layer. T. Sreenivasulu and BVSSS Prasad (2011)[7] identified sweeping , mixing flows and hot spots regions of a seven bundle and presented geometric parametric investigations for a wide Reynolds number range using commercial CFD code. Jae-ho Jeong et al. (2015)[8] analyzed complicated and vortical flow phenomena in a wire-wrapped 37-pin fuel bundle for SFR using CFX. They also discussed the effects of the driving forces on the wire spacer. M. Naveen Raj and K. Velusamy (2016)[9] studied transverse and axial flow pattern and heat transfer characteristics in different subchannels of a 217 pin wire wrapped bundle by CFD solver. However, the research on the complex flow and heat transfer in the wire-wrapped subassembly is still limited. The mesh modeling and computation resource are challenges in most of the numerical simulations.

In the present study, with an effort to reduce the required computational grids and modeling time, a new structured mesh generation method is developed for the wire-wrapped fuel bundle using special mesh marked and separated strategies. The simulation method was firstly

validated through the 19-pin wire-wrapped fuel assembly experimental data. And then three-dimensional flow and heat transfer fields of the 61-pin fuel subassembly for CEFR were numerically investigated using the commercial CFD code, Fluent. Complicated local axial and transverse flow phenomena in the interior, edge and corner subchannels were quantitatively analyzed.

II. NUMERICAL METHOD

1. Governing equations

The three-dimensional conservation equations that govern steady and incompressible flow and heat transfer are employed and expressed as follows[10]:

Continuity:

$$\nabla \cdot (\rho \vec{v}) = 0 \tag{1}$$

Momentum:

$$\nabla \cdot (\rho \vec{v}\vec{v}) = -\nabla p + \nabla \cdot (\bar{\bar{\tau}}) + \rho \vec{g} + \vec{F} \tag{2}$$

where

$$\bar{\bar{\tau}} = \mu[(\nabla \vec{v} + \nabla \vec{v}^{T}) - \frac{2}{3}\nabla \cdot \vec{v} \cdot I] \tag{3}$$

Energy:

$$\nabla \cdot (\vec{v}(\rho E + p)) = \nabla \cdot (k_{eff} \nabla T - \sum_{j} h_j \vec{J}_j + (\bar{\bar{\tau}}_{eff} \cdot \vec{v})) + S_h \tag{4}$$

where

$$E = h - \frac{p}{\rho} + \frac{v^2}{2} \tag{5}$$

Turbulence is modeled by the realizable k–ε model and the transport equations are:

Turbulent kinetic energy (k):

$$\frac{\partial}{\partial t}(\rho k) + \frac{\partial}{\partial x_j}(\rho k u_j) = \frac{\partial}{\partial x_j}[(\mu + \frac{\mu_t}{\sigma_k})\frac{\partial k}{\partial x_j}] + G_k + G_b - \rho\varepsilon - Y_M + S_k \tag{6}$$

Turbulent dissipation rate (ε):

$$\frac{\partial}{\partial t}(\rho \varepsilon) + \frac{\partial}{\partial x_j}(\rho \varepsilon u_j) = \frac{\partial}{\partial x_j}[(\mu + \frac{\mu_t}{\sigma_\varepsilon})\frac{\partial \varepsilon}{\partial x_j}] + \rho C_1 S \varepsilon - \rho C_2 \frac{\varepsilon^2}{k + \sqrt{v\varepsilon}} + C_{1\varepsilon}\frac{\varepsilon}{k} C_{3\varepsilon} G_b + S_\varepsilon \tag{7}$$

where

$$C_1 = \max[0.43, \frac{\eta}{\eta + 5}] \tag{8}$$

$$\eta = S\frac{k}{\varepsilon} \tag{9}$$

$$S = \sqrt{2 S_{ij} S_{ij}} \tag{10}$$

where G_k is the generation of turbulence kinetic energy due to the mean velocity gradients, G_b indicates the generation of turbulence kinetic energy caused by buoyancy, σ_k and σ_ε are the turbulent Prandtl numbers for k and ε, respectively, S_k and S_ε represent user-defined source terms.

The standard wall functions is adopted in the present simulation as follows:

$$U^* = \frac{1}{\kappa}\ln(E y^*) \tag{11}$$

where U^* is the dimensionless velocity given as:

$$U^* \equiv \frac{U_P C_\mu^{1/4} \kappa_P^{1/2}}{\tau_w / \rho} \tag{12}$$

and y^* indicates the dimensionless distance from the wall

$$y^* \equiv \frac{\rho C_\mu^{1/4} \kappa_P^{1/2} y_P}{\mu} \tag{13}$$

The non-dimenaional wall distance y^+ is defined as follows:

$$y^+ \equiv \frac{\rho u_\tau y}{\mu} = \frac{\rho y}{\mu}\sqrt{\frac{\tau_w}{\rho}} \tag{14}$$

On the basis of the recommended guidance in the CFD code theory guide, when the y+ lies higher than laminar sub-layer limit of 30, the wall function is suitable. For the mesh chosen in the present simulation, the average near wall y+ is 63.

2. Geometry and mesh generation

The 61-pin wire-wrapped fuel assembly of CEFR is simulated in the present work as shown in Fig.1., which consists of triangular-arrayed fuel pins, helical wire wrappers and hexagonal duct. Table I. lists the Geometric parameter values of computational model. The fuel assembly has an active portion that is 450mm long, with a hexagonal duct of 56.6mm in width across flat[11]. Fuel pin is 6 mm in diameter and 6.95mm in pitch, which is helically wrapped by wire spacers (0.95 mm in diameter and 100mm in a wire pitch). These wire wrappers nearly tangent to fuel pin surfaces provides fastening and spacing, as well as increasing the flow mixing between gaps formed by the fuel pins. The simulation contains 4.5 pitch heights of the pin bundle.

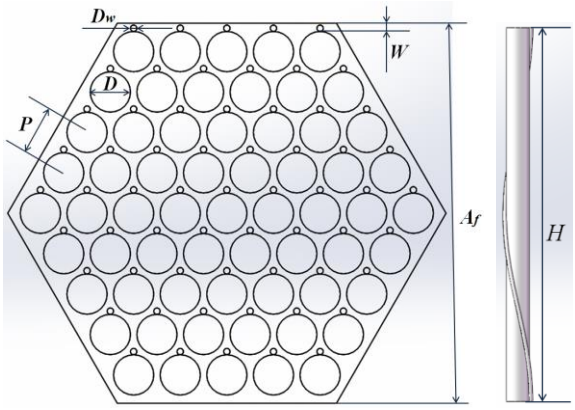

Fig. 1. Geometry configuration of 61-pin wire-wrapped fuel assembly.

Table I. Geometric parameter values

Parameter	Length(mm)
Lead-to-diameter ratio *H*/*D*	16.667
Pitch-to-diameter ratio *P*/*D*	1.158
Outer diameter *D*	6
Triangular Pitch *P*	6.95
Length *L*	450
Wire diameter D_w	0.95
Wire pitch *H*	100
Width across flats A_f	56.6
Width *W*	4.224

Due to the intricate geometry of the wire-wrapped assembly, a huge number of mesh cells is required, as well as much computational time. For the adequate prediction of field variables such as secondary flows, high performance computers are generally demanded to generate the mesh. In the present study, a new mesh generation method was developed to employ high quality hexahedral mesh with nonuniform density, so as to avoid a large amount of tetrahedral mesh and reduce the modeling time.

Firstly, the structured hexahedral mesh of the fuel subassembly without wire wrappers has been generated using the software ICEM CFD. According to the geometric periodicity, six topologically blocks associated to the space around a fuel pin can be rotated and copied to cover all the bundle region or the mesh around one pin can also be pasted to obtain the entire domain mesh. The blocks and hexahedral mesh are shown in Fig. 2, where the dense mesh areas are concentrated near the pin walls. The structured hexahedral mesh shows a good quality of greater than 0.65 and a relatively rapid generating speed. The second step is dealing with the mesh of helical spacer wires by some techniques and functions provided in the CFD code Fluent. Locus equations of wire wrappers are written in the user defined functions as follows:

$$x = A\cos\theta \tag{15}$$

$$y = A\sin\theta \tag{16}$$

$$z = \frac{H}{2\pi}\theta \tag{17}$$

where

$$\theta = y \cdot 2\pi / H \tag{18}$$

And then the wire spacers mesh can be marked in the user defined memory and separated from the whole mesh domain. Fig. 3. presents the separated mesh of all the wire wrappers. In the most previous research, the wire wrapper is changed to be linearly attached to the pin wall by moving the wire location or increasing the wire diameter to avoid point contact in two dimensions. Due to the wire wrapper is marked by locus equations and separated from the mesh, the real geometry of wire-wrapped fuel subassembly could be maintained as far as possible in the present simulation. The final required calculational mesh with spacer wires deleted is shown in Fig. 4. This mesh technique is obviously different from the conventional mesh method. With no need to create geometry and generate mesh with the wire wrapper, the new method can easily obtain the complex mesh of wire wrappers and change the geometric parameters in the locus equations to perform the fuel assembly design study.

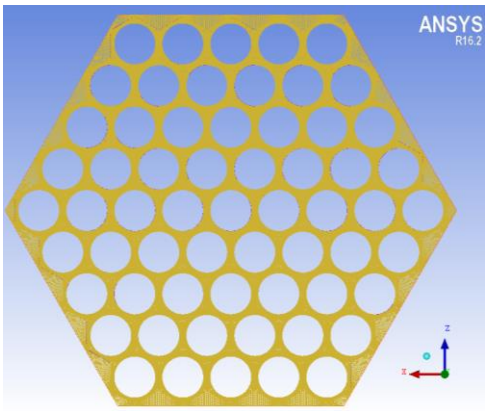

(a) Original mesh distribution in a cross-section plane

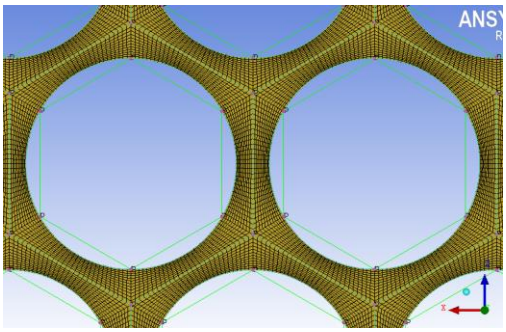

(b) Mesh distribution between two pin walls

Fig. 2. Original mesh distribution without wire wrappers of 61-pin wire-wrapped fuel subassembly

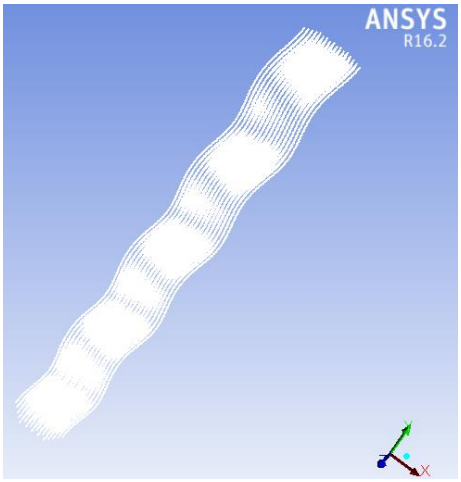

Fig. 3. Separated mesh of all the wire wrappers

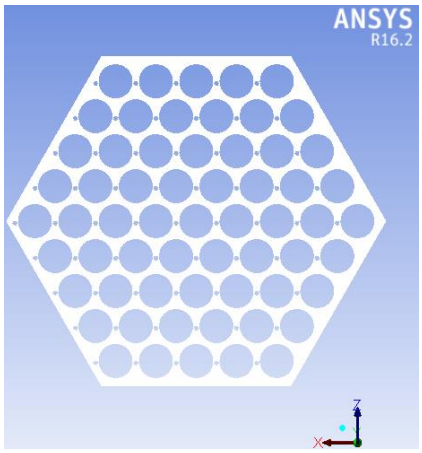

Fig. 4. Final mesh distribution in a cross-section plane of 61-pin wire-wrapped fuel subassembly

3. Boundary conditions and simulation models

Boundary conditions are present in Fig.5. Sodium properties at an averaged temperature744K were specified. Inlet temperature and velocity were specified at 633.15 K and 4.5 m/s, respectively. A static pressure 0 Pa was set at the bundle outlet. Constant heat flux of 1872.559 kW/m^2 was imposed on the fuel pin walls ,while the wire wrapper and hexcan surfaces were taken to be adiabatic. No slip boundary condition is applied on all solid walls. The turbulence parameters in boundary conditions, 2.655mm for hydraulic diameter and 4.34% for turbulence intensity, were calculated and adopted.

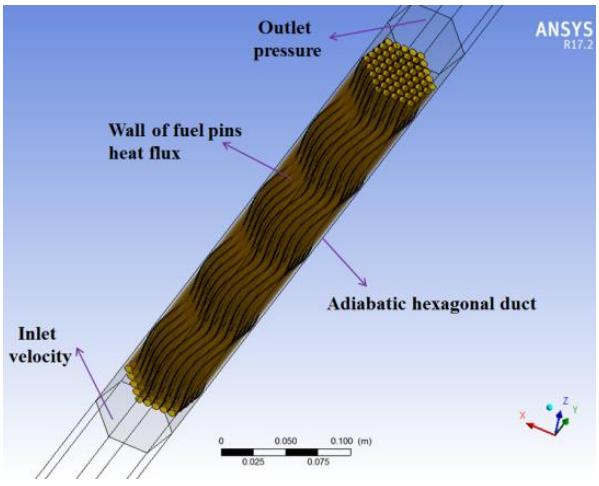

Fig. 5. Calculational boundary conditions

The SIMPLE scheme was selected for pressure-velocity coupling. Second-order scheme was used for the discretization of governing equations. Reynolds number was 33880 and the realizable k–ε model with standard wall functions was applied in the simulation. The average outlet

temperature and mass flow rates of different cross sections including inlet and outlet were monitored in the iterative process. When the residual values for the continuity, momentum and transport equations reach 10^{-7}, 10^{-8} and 10^{-6}, respectively, and all the monitor variables were constant, the convergence is declared.

4. Grid independency study

As shown in Table II, the grid independency study was performed for the 61-pin wire-wrapped fuel subassembly with 4.5 helical pitches in two steps . Firstly, the number of radial mesh between two adjacent fuel pin walls was set to be 26. Three different axial grid configurations (named A1, A2, A3) were chosen. The averaged outlet temperature was taken as the target variable and deviations were made by comparing the result with that of the fine mesh A3. Similarly, the number of axial mesh points was fixed at 151 in all different radial meshes R1, R3 and R3 in the next step. It can be seen that results of mesh configuration A2 and R2 were very close to those of fine mesh A3 and R3, respectively, which can be considered as a nearly grid independent solution. Therefore, the mesh with 151 axial points and 26 divisions around the adjacent radial distance of two fuel pin walls was selected in the present simulation, which has a total cells number of 19.35 millions .

Table II. The grid independency study for the 61-pin wire-wrapped subassembly

The axial grid was changed (the number of radial mesh was fixed at 26)		
Grid name	No. of axial mesh point	No. of mesh cells(millions)
A1	91	11.62
A2	151	19.35
A3	201	25.8
	Averaged outlet temperature	Deviation with fine mesh A3 (%)
A1	828.97	-0.092
A2	829.61	-0.014
A3	829.73	---
The radial grid was changed (the number of axial mesh was fixed at 151)		
Grid name	No. of radial mesh point	No. of mesh cells(millions)
R1	22	17.19
R2	26	19.35
R3	38	29.93
	Averaged outlet temperature	Deviation with fine mesh R3 (%)
R1	825.96	-0.52
R2	829.61	-0.081
R3	830.28	---

5. Validation calculation

In order to check the accuracy, the numerical method is validated by calculating 19-pin wire-wrapped fuel assembly experiment performed by Moon-Hyun Chun[12]. The test section B2 of the 19-pin assembly was 1300mm in length with a helical pitch height of 200mm. Pins of 8mm in diameter were arranged in triangular configuration with a pitch of 10.04mm and the wire diameter was 2 mm. Pressure drops were measured and a series of friction factors were obtained in the water experiment. As shown in Table III, the predicted friction factors agree well with experimental data in a wide range of Reynolds number. For the laminar region (defined by the Cheng and Todreas correlation[13]), the CFD predicted values generally lower than the experimental data, contrary to results for the turbulent region. It is seen that the maximum deviation is 6.66% .

Table III. Comparison of friction factors from experiment and CFD calculation

Reynolds	$f_{experimental}$	f_{CFD}	%error
356.52	0.265473	0.263908	-0.59
723.39	0.145954	0.14442	-1.05
5556.37	0.05109	0.05276	3.27
26735.19	0.031623	0.033729	6.66
35651.95	0.030227	0.031201	3.22

III. RESULTS

To quantitatively analyze the complex local flow features, the subassembly has to be divided into various regions. As depicted in Fig. 6., three types of subchannels were chosen, named interior , edge and corner subchannel, respectively.

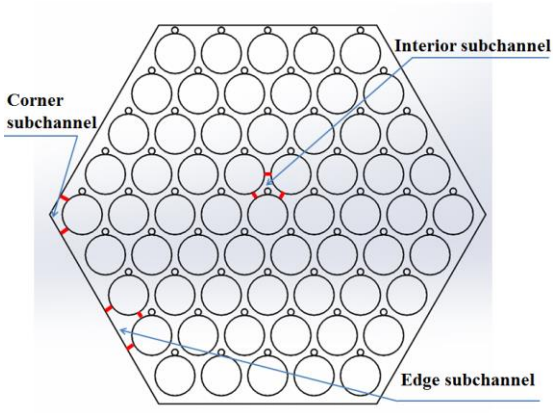

Fig. 6. Location of three types of subchannels chosen in the present study

1. Three-dimensional temperature field

As shown in Fig. 7., the temperature in different cross-sectional planes increases with axial height. In the same cross-sectional plane, the sodium temperature is higher in interior zones compared with that in peripheral and corner regions. The reason can be attributed as follows: the heat is applied on the fuel pin walls, while hexagonal duct surfaces are set to be adiabatic. The average outlet temperature of the entire subassembly is 831.6K. Fig. 8. depicts area-averaged temperature distribution at various axial positions. It can be seen that the average temperature in the edge and corner subchannels presents nonlinear variation with axial height. The average outlet temperature of the interior , edge and corner subchannel is 908.2K, 773.7K and 762.8K, respectively.

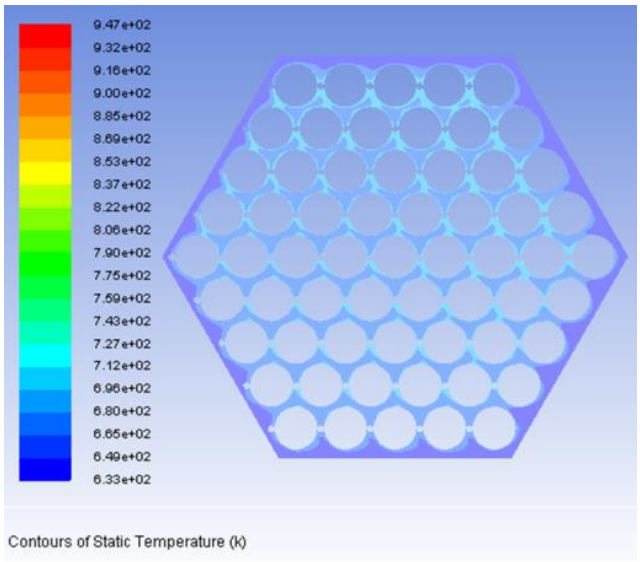

(a) y=0.05m

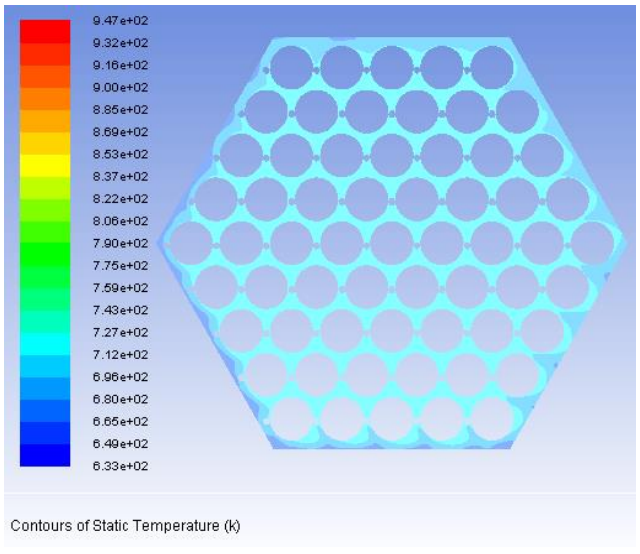

(b) y=0.15m

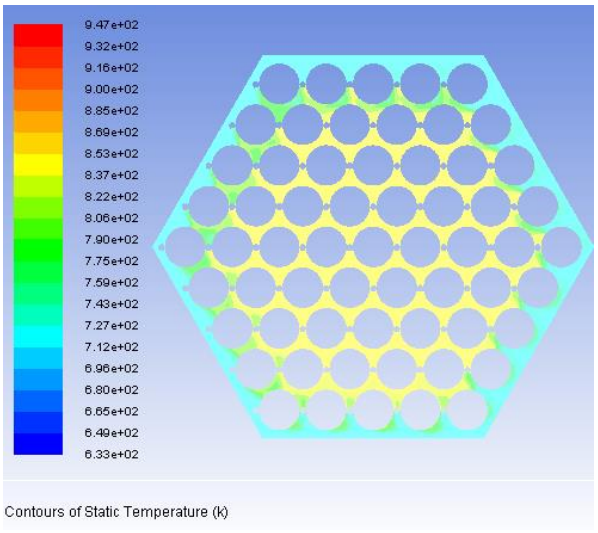

(c) y=0.35m

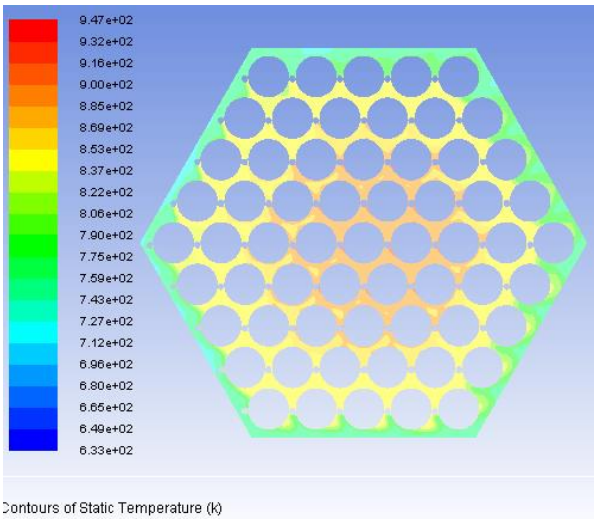

(d) y=0.45m

Fig. 7. Temperature distribution in different cross-sectional planes

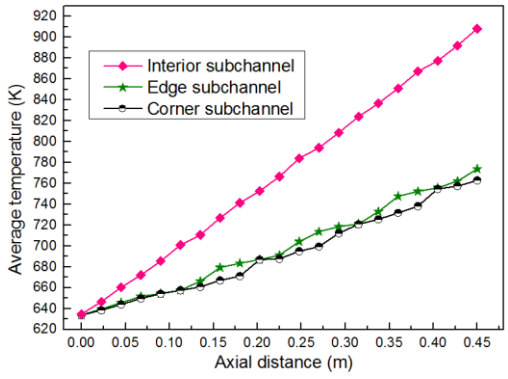

Fig. 8. Average temperature distribution along axial heights in different subchannels

2. Three-dimensional flow field

Fig. 9 shows velocity distribution in different cross-sectional planes of y=0.35 m, 0.375 m, 0.4 m and 0.425 m. Since the spacer wires are helically wrapped on the fuel pins along the axial direction, periodic velocity variation has been observed in different cross-sectional planes. As the coolant flows upward in the bundle, the region of maximum velocity shifts from one cross section to the subsequent one. Furthermore, owing to the differences in flow area, hydraulic resistance and orientation of wire spacers, velocity distribution in the same plane is nonuniform. The velocity in the edge and corner zones is higher than that in the interior region. Different subchannels have a relative position related to the wire wrappers and hexagonal duct surfaces, which imposes an effect on the three-dimensional flow characteristics.

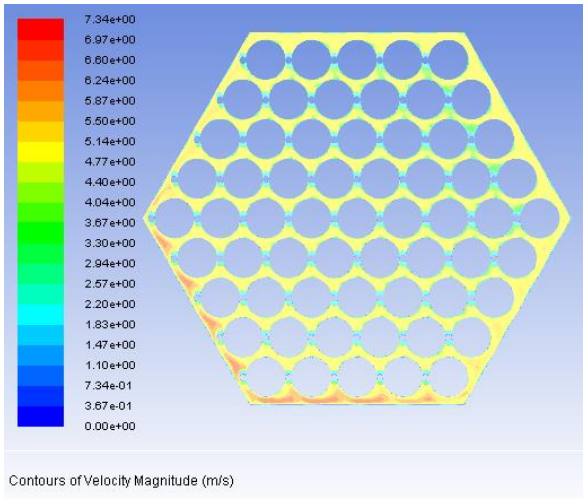

(a) y=0.35m

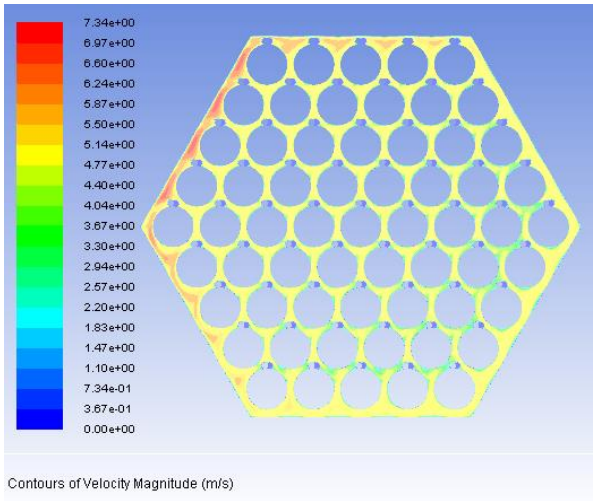

(b) y=0.375m

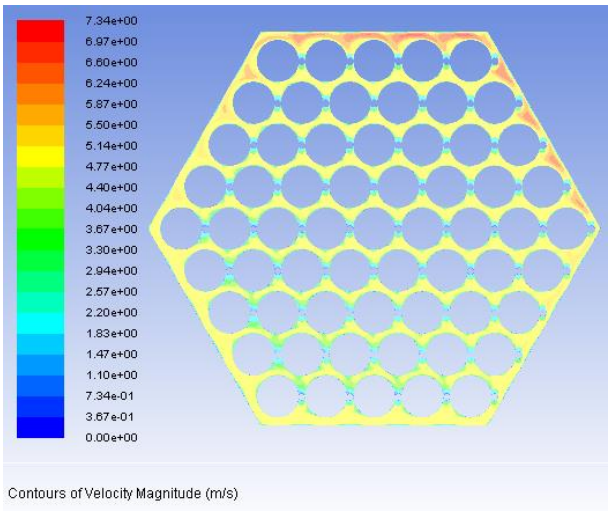

(c) y=0.4m

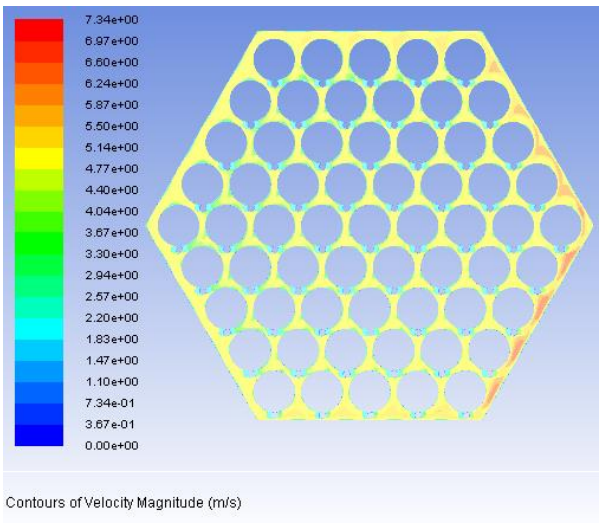

(d) y=0.425m

Fig. 9. Velocity distribution in different cross-sectional planes

As depicted in Fig. 10., obvious spatially oscillating flow exists within each subchannel, which results from the presence of helical wire wrappers. The phase and amplitude of flow oscillations in the corner and edge subchannels present similar distribution, while the flow in interior subchannel has smaller phase and amplitude. The peak average velocity magnitude in the edge subchannel reaches 6.35 m/s. The average velocity magnitude in the corner, edge and interior subchannel is about 1.178, 1.176 and 0.98 times of the inlet velocity 4.5 m/s, respectively.

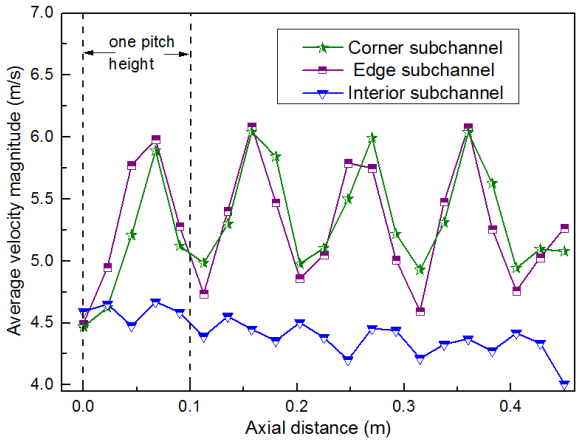

Fig. 10. Average velocity magnitude at various axial locations in different subchannels

Fig.11 and Fig.12 show pressure distributions in the plane y=0.325m and x=0m, respectively. Since fuel pins are helically wound with wire wraps, the pressure display nonuniform distribution in both cross section and axial direction section. The average pressure drop in the whole bundle domain is 46.8 kPa.

Fig. 13 depicts vector contour of velocity component z in different subchannels. It can be seen that there exists a clockwise transverse swirl flow around the pin walls, which is in the direction same as that of wire wrappers rotation.

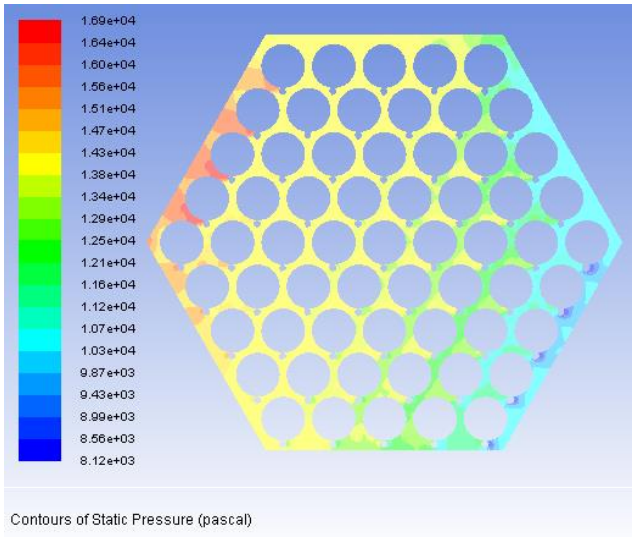

Fig. 11. Pressure distribution in the cross-sectional plane y=0.325m

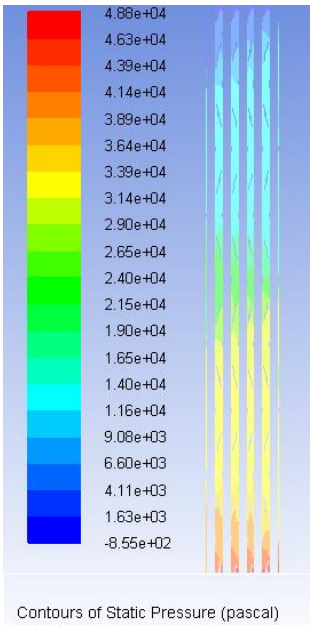

Fig. 12. Pressure distribution in the plane x=0m

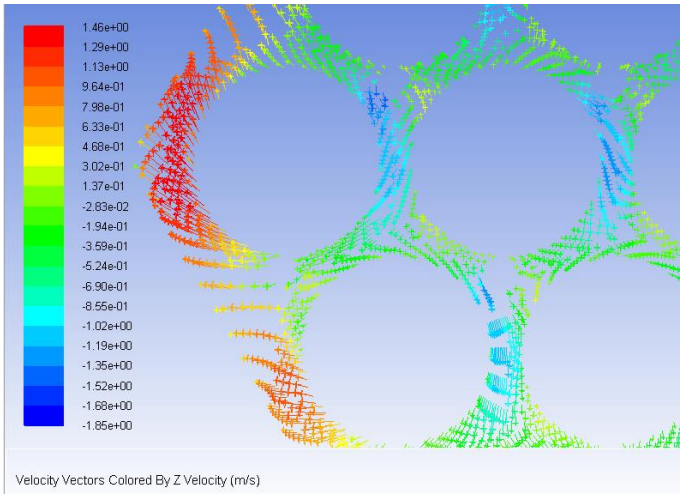

Fig. 13. Vector contour of velocity component z in different subchannels

3. Different subchannel flow behaviors

The axial and transverse flow behaviors in the interior, edge and corner subchannels have been investigated in the present simulation. The average axial velocity v within 1.4 pitch heights in different subchannels is plotted in Fig. 14. Axial flow characteristic of spatially oscillating in the edge subchannel is nearly similar to that of the corner subchannel, which has a periodicity of one pitch height. The average axial velocity in the edge and corner subchannels is about 23% higher than that in the interior subchannel. In addition, it can be noted that within an axial length of one pitch height, the interior subchannel is formed with three wire

wrappers wrapped on three fuel pins. Hence, the average axial velocity in the interior subchannel periodically changes and attains three peak values within one pitch.

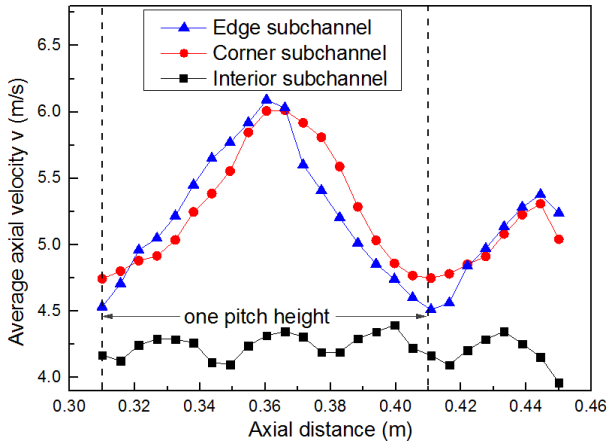

Fig. 14. Average axial velocity v within 1.4 pitch heights in different subchannels

Average velocity component u and w (transverse flow) also exhibit spatial fluctuation phenomena shown in Fig.15 and Fig.16 . The amplitude and phase shift of flow fluctuation is quite distinct in the interior, edge and corner subchannels. Transverse flow behaviors of different subchannels are closely related to the rotation direction of wire wrappers and relative position between the wires and hexagonal walls. The cross flow mixing induced by helical wires has a positive effect on uniform temperature distribution in the subassembly. This cross flow effect could promote the convective heat transfer and reduces the peak coolant temperature.

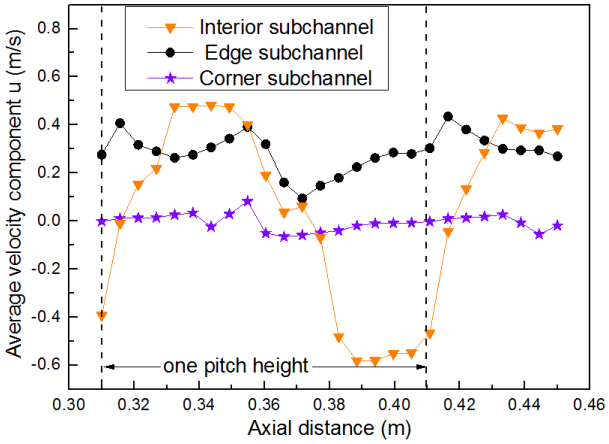

Fig. 15. Average velocity component u within 1.4 pitchs height in different subchannels

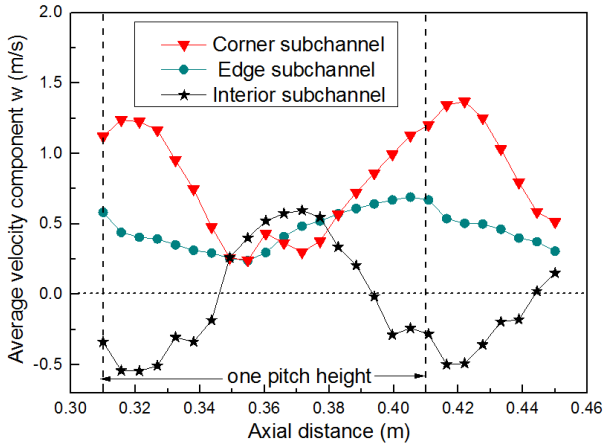

Fig.16. Average velocity component w within 1.4 pitchs height in different subchannels

The area-averaged transverse velocity U_t can be normalized by the the inlet axial velocity 4.5 m/s as:

$$U_N = \frac{U_t}{v_{in}} = \frac{\sqrt{u^2 + w^2}}{v_{in}} \tag{19}$$

The normalized average transverse velocity U_N within 1.4 pitch heights in different subchannels is depicted in Fig.17. The transverse velocity fluctuation is more dominant in the corner subchannel. Wire wrappers induce a maximum transverse flow velocity of about 30% of inlet axial velocity. The transverse flow effect in the corner and edge subchannels is stronger than that in the interior subchannel.

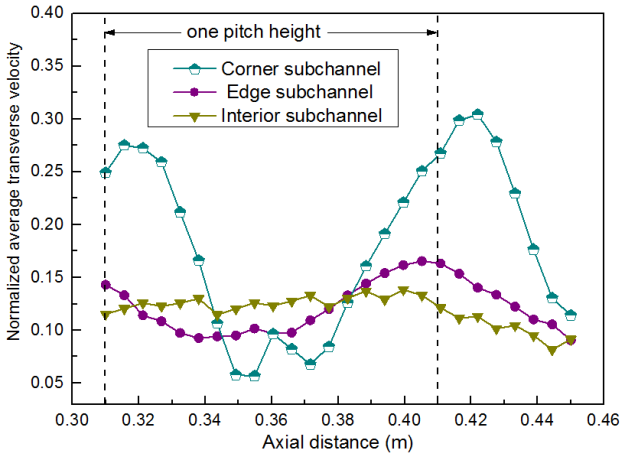

Fig.17. Normalized average transverse velocity within 1.4 pitch heights in different subchannels

IV. CONCLUSIONS

Three-dimensional numerical analysis of a 61-pin wire-wrapped fuel subassembly has been carried out. In the present study, a reliable new mesh generation method was proposed with reasonable cost and local flow characteristics in the subassembly were captured. The following conclusions can be drawn:

The average temperature in the edge and corner subchannel exhibits nonlinear variation with axial height. Periodic velocity variations have been observed in the subassembly. The velocity magnitude in the edge and corner zones is higher than that in the interior region.

Distinct axial and transverse flow characteristics in different subchannels result from the flow area, hydraulic resistance and orientation of wire spacers. The average axial velocity in the edge and corner subchannels is about 23% higher than that in the interior subchannel. The maximum transverse flow velocity is about 30% of inlet axial velocity. The transverse flow in corner and edge subchannels is stronger than that in the interior subchannel. Further, there are one oscillation peak of the average axial velocity in the edge and corner subchannels within one pitch, while three axial velocity peaks occur in the interior subchannel.

This simulation approach with special mesh techniques could be extended to investigate the flow and heat transfer features and perform design analysis of 217-pin wire-wrapped fuel subassembly in the future work.

NOMENCLATURE

A = distance between the center of the fuel fin and wire wrap center
H = wire pitch
u = velocity component in the x direction
U_N = normalized average transverse velocity
U_t = transverse velocity
v = velocity component in the y direction (axial velocity)
v_{in} = inlet axial velocity
w = velocity component in the z direction

ACKNOWLEDGMENTS

This work was supported by National Natural Science Foundation of China (Grant No. 11605131).

REFERENCES

1. Wei Wang. The introduction of chinese demonstration fast reactor project[J]. Nuclear safety, 2011, 2:76-78.
2. IAEA. Status of Fast Reactor Research and Technology Development [R]. IAEA-TECDOC-1691. Vienna : International Atomic Energy Agency, 2012.
3. Kazumi Aoto, Philippe Dufour, Yang Hongyi, et al. A summary of sodium-cooled fast reactor development[J]. Progress in Nuclear Energy,77(2014):247-265.
4. Raza W, Kim K Y. Comparative analysis of flow and convective heat transfer between 7-pin and 19-pin wire-wrapped fuel assemblies[J]. Journal of Nuclear Science and Technology, 2008, 45(7): 653-661.
5. Pointer W D, Thomas J, Fanning T, et al. RANS-based CFD simulations of sodium fast reactor wire-wrapped pin bundles[J]. Proceedings of M&C, 2009, 9.
6. Hamman K D, Berry R A. A CFD simulation process for fast reactor fuel assemblies[J]. Nuclear Engineering and Design, 2010, 240(9): 2304-2312.
7. Sreenivasulu C T, Prasad C B. Flow and heat transfer characteristics in a seven tube-bundle wrapped with helical wires[J]. International Journal of Advancements in Technology, 2011.
8. Jeong J H, Yoo J, Lee K L, et al. Three-dimensional flow phenomena in a wire-wrapped 37-pin fuel bundle for SFR[J]. Nuclear Engineering and Technology, 2015, 47(5): 523-533.
9. Raj M N, Velusamy K. Characterization of velocity and temperature fields in a 217 pin wire wrapped fuel bundle of sodium cooled fast reactor[J]. Annals of Nuclear Energy, 2016, 87: 331-349.
10. ANSYS, 2009. Ansys Fluent 12.0 Theory Guide. Fluent Inc., Lebanon, NH.
11. Yizhe Liu, Yu Hong. Thermal-hydraulic analysis of fuel subassemblies for sodium cooled fast reactor [J]. Atomic Energy Science and Technology, 2008, 42(2): 128-134.
12. Chun Moon-Hyun, Kyong-Won Seo. An experimental study and assessment of existing friction factor correlations for wire-wrapped fuel assemblies [J]. Annals of Nuclear Energy, 17 (2001): 1683-1695.
13. Cheng S K, Todreas N E. Hydrodynamic models and correlations for bare and wire-wrapped hexagonal rod bundles—bundle friction factors, subchannel friction factors and mixing parameters[J]. Nuclear engineering and design, 1986, 92(2): 227-251.